ISABE 2007-1280

Optical Measurements in a Combustor Using a 9-Point Swirl-Venturi Fuel Injector

Yolanda R. Hicks and Robert C. Anderson
NASA Glenn Research Center
Cleveland, Ohio USA
Randy J. Locke
ASRC Aerospace
Cleveland, Ohio USA

ABSTRACT

This paper highlights the use of two-dimensional data to characterize a multipoint swirl-venturi injector. The injector is based on a NASA-conceived lean direct injection concept. Using a variety of advanced optical diagnostic techniques, we examine the flows resultant from multipoint, lean-direct injectors that have nine injection sites arranged in a 3 x 3 grid. The measurements are made within an optically-accessible, jet-A-fueled, 76-mm by 76-mm flame tube combustor. Combustion species mapping and velocity measurements are obtained using planar laser-induced fluorescence of OH and fuel, planar laser scatter of liquid fuel, chemiluminescence from CH*, NO*, and OH*, and particle image velocimetry of seeded air (non-fueled). These measurements are used to study fuel injection, mixedness, and combustion processes and are part of a database of measurements that will be used for validating computational combustion models.

NOMENCLATURE

Symbols

CH*	[-]	CH radical
OH*	[-]	hydroxyl radical
NO*	[-]	nitric oxide radical
CO	[-]	carbon monoxide
P	[kPa]	pressure
T	[K]	temperature
Φ	[-]	equivalence ratio
f	[mm]	focal length
ΔP/P	[-]	combustor pressure drop
L/D	[-]	length-to-diameter ratio

Abbreviations

MP-LDI	Multipoint Lean Direct Injection
LTO	Engine Landing-Take-Off Cycle
NCC	National Combustion Code
PLIF	Planar Laser-Induced Fluorescence
PLS	Planar Laser Scattering
PIV	Particle Image Velocimetry
ICCD	Intensified Charge Coupled Device
CFD	Computational Fluid Dynamics
RANS	Reynolds-Averaged Navier Stokes

INTRODUCTION

Multipoint Lean Direct Injection (MP-LDI) is an injection concept that has proved a viable candidate for reduced emissions [1-3]. The LDI injector concept is a new generation liquid fuel injector developed to reduce aircraft NO_x emissions, and later modified to exceed the 1996 International Civil Aviation Organization standards while maintaining CO and unburnt hydrocarbons at current levels. It is designed to rapidly mix fuel and air so that stable combustion occurs within a short distance. Swirl is imparted to the air to generate recirculation zones that anchor the flame(s) near the fuel injection sites, as shown conceptually in figure 1. This concept allows for many small fuel injectors integrated into modules so that there are several flame zones within a combustor. This allows for a variety of fuel staging possibilities appropriate for an LTO engine cycle. Because the concept provides low emissions, allows for different fuel staging strategies, and has realistic, complex fluid interactions, the MP-LDI concept was chosen as our primary fuel injector/mixer test case for validating the National Combustion Code (NCC).

To assess and validate the NCC, it is necessary to obtain a comprehensive measurement database to fully characterize the injector for a range of operational conditions. Parameters that need to be investigated include fuel drop size, liquid and gas phase velocity, combustion temperature distribution, and concentration profiles for both major and minor species. To begin building a validation database, we tested a 9-point MP-LDI injector in the NASA Glenn CE-5 flame tube combustor facility using several optical diagnostic methods. Optical methods are the only means that provide the spatial resolution required for a validation dataset. Sampled gas emission probes are generally restricted to

certain fixed locations within the combustor, whereas the locations of optical probes are only limited by the optical access. Thus, high-resolution, optically-acquired sampling can extend from immediately downstream of the fuel injector exit plane, through the high-temperature flame zone, to locations where gas samples are typically obtained from 100-mm to 200-mm downstream of the injector exit. Additionally, optical diagnostics avoid the undesirable flow perturbations that result from using standard gas sampling probes. For these tests the inlet conditions ranged in temperature from 505 K to 830 K and in pressure from 690 kPa – 1720 kPa. The fuel-to-air equivalence ratio (ϕ) was varied from 0.35 to 0.5. In order to test realistic conditions for this injector the test matrix included conditions that allow us to examine the effects of fuel staging. We obtained two-dimensional species distributions of liquid fuel, fuel vapor, and hydroxyl radical for several inlet conditions via planar laser-induced fluorescence (PLIF), planar laser scattering (PLS), and chemiluminescence methods. We measured air velocity using 2-D particle image velocimetry (PIV). Additionally, we acquired flame visualization data using both standard video and high speed imaging, with frame rates up to 16-kHz. These experiments mark the first time NCC validation data have been acquired under realistic conditions, and the first-ever use of PIV in our combustor facility.

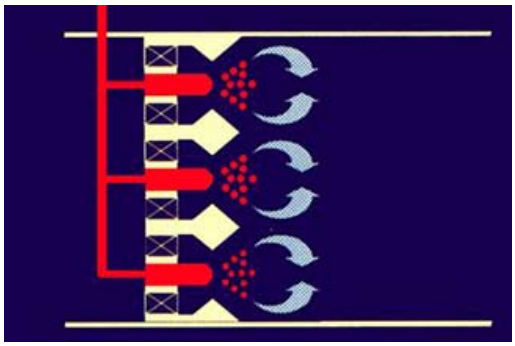

Figure 1. Conceptual sketch showing the LDI concept.

EXPERIMENTAL SETUP

Injector Hardware

Figure 2 is a photograph showing the end-view of the 9-point LDI injector assembly from the perspective of aft looking forward. The photograph displays the relative placement of the individual injectors with corresponding swirlers. The injectors are spaced on one inch (25.4-mm) centers and the swirlers impart a clockwise (stream-wise) rotation to the flow. The overall flow path dimension is 76.2-mm by 76.2-mm (3-in x 3-in). Each of the nine elements of the array is comprised of a simplex nozzle, an axial swirler, and a converging-diverging venturi. The swirler has six vanes angled at 60° relative to the main flow direction. The swirler sits just upstream of the fuel nozzle, whose exit is at the throat of the venturi. The fuel is atomized as it exits the injector tip.

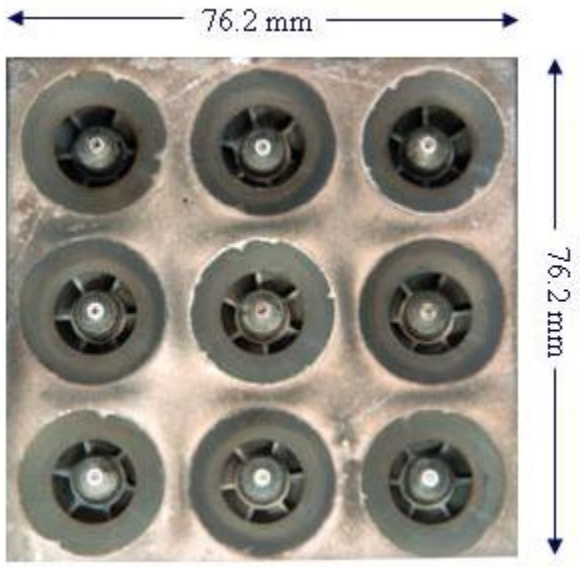

Figure 2. Photograph of the 9-pt LDI injector. The view is aft looking forward.

These details are illustrated in the schematic drawing in figure 3 for a single injection element, or point. Further details of this particular test hardware can be found in reference [3].

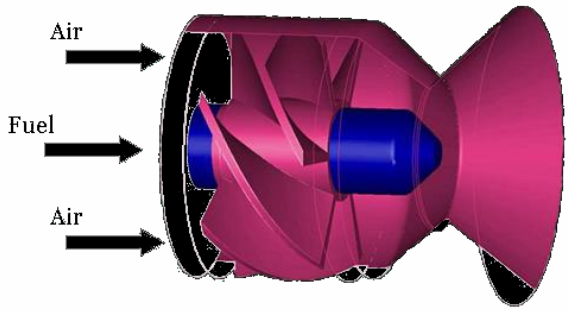

Figure 3. Schematic drawing showing the relative spatial positioning of the air swirler, fuel nozzle, and venturi for each injector element.

Diagnostics Setup and Procedure

The 9-point LDI injector is mounted in an optically-accessible flame tube combustor that has four windows mounted in the sides of the square flow path. The combustor facility is designed so that the core flow travels horizontally. The UV-grade fused silica windows provide a clear aperture of 38.1 mm in the axial direction and

50.8-mm in the orthogonal horizontal and vertical directions. Therefore, the field-of-view provided when looking perpendicular to the flow is 67% of the total chamber height.

The imaging results reported here were acquired using a similar physical arrangement to that illustrated in figure 4. The probe laser light is formed into a sheet and directed through the flow field at the desired location. A camera focused at the location of the laser sheet is positioned to collect either the light scattered elastically (for PLS and PIV) from fuel drops or particles, or fluoresced (for PLIF) from specific molecular species. The laser sheet and camera are traversed across the flow using high-precision, motorized stages.

PLIF and PLS data are acquired using a 10-Hz Nd:YAG/dye laser system and intensified, gated CCD (ICCD) cameras. Two ICCD cameras are used, located on opposite sides of the combustor. Light is collected using f = 105-mm, f/4.5 UV grade camera lenses. To pass the appropriate light through these lenses, we use narrow band filters to allow the capture of a particular band of fluorescent wavelengths for fuel and OH PLIF, and a line filter to collect the elastically-scattered light for PLS. We can select the appropriate filter using five-position filter wheels. The laser sheet and camera are traversed across the flow in 1-mm increments. The images from a traverse are formed into a three-dimensional data block. The light is collected typically as on-chip integrated averages of 50 shots. A series of 100 single-shot images were also collected for each inlet condition to investigate shot-to-shot variations. Chemiluminescence images of CH*, NO*, and OH* from the bulk fluid were collected with the camera focused on the center plane, using the appropriate filter. These data were also collected in gated mode, collecting 200 on-chip integrated averages.

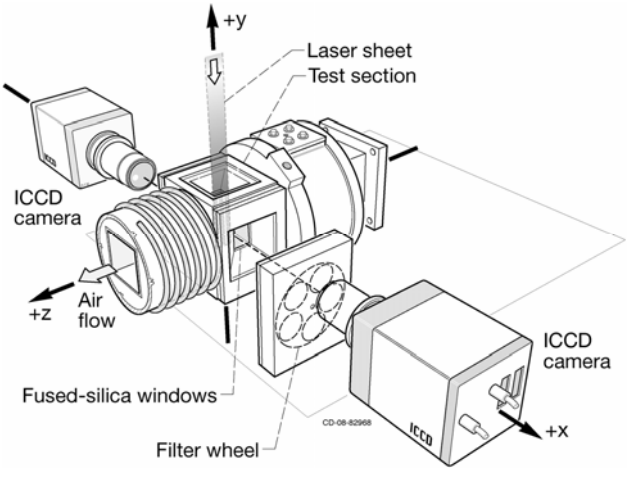

Figure 4. Schematic drawing illustrating the relative orientation of the laser sheet and cameras to the test rig for a vertically-applied laser sheet.

The PIV data were acquired using a 15-Hz double-head Nd:YAG laser and a single CCD camera. Because this is a 2-D system, we ran our tests once using a vertical laser sheet and again with a horizontal laser sheet. We traversed across the flow in 3-mm increments. The particles used to obtain the velocity data were 0.3-micron diameter aluminum oxide particles that were seeded into the air inlet plenum 10-L/D before the plenum exit. The inlet plenum feeds the flow to the flame tube test section.

EXPERIMENTAL RESULTS

Two-dimensional species contour maps showing the distribution of total fuel, OH* and liquid fuel were derived from PLIF and PLS data. Examples of these data are shown in figure 5 and figure 6, which show end views of fuel PLIF (left), OH PLIF (center), and PLS from fuel droplets (right) 7.5 mm downstream from the injector exit plane. The black circles and partial circles indicate the positions of the nine injector diffuser exits. Because the field of view afforded us by our windows does not encompass the entire flow field, only the center injector can be seen completely whereas only half of the top, bottom and two side injectors are visible; and one-quarter of the four corner injectors are visible. Each image shown is derived from its corresponding data block, which incorporates all the image data within the optically-accessible volume. Each species data block is scaled independently, so the relative intensity levels of the three species maps cannot be directly compared.

The planar OH PLIF data showed evidence of attenuation of the excitation laser from top to bottom. Neither the fuel PLIF nor the PLS data showed significant attenuation effects. Therefore, in the images shown here, the OH data has been corrected. To achieve the correction, the assumption was made that the laser energy would decay exponentially as it passed from top to bottom through the flow. The vertical profile was used with a curve fitting routine to develop an estimate of the attenuation function. The attenuation estimate was then used to correct the data pixels based on their vertical position in the data block. The exponential function was chosen based on the assumption that the attenuation would follow the well-know Beer-Lambert Law. We recognize that the Beer-Lambert Law assumption of a homogeneous mixture may be violated in this case. Similarly a correction was performed in the horizontal direction. However, the attenuation estimate used was linear in this case because the attenuation in this case is likely due to scattering effects, not absorption. A more rigorous correction algorithm will be considered in future work.

Higher concentrations of OH*, which denote flame location, are shown in shades of blue; the corresponding fuel images indicate relatively lower concentrations predominantly in reds and yellows because most of the

fuel (liquid or vapor) has reacted at this distance downstream.

The inlet conditions for the images shown in figure 5 are T_{in} = 617K, P_{in} = 1034 kPa, ϕ = 0.38; and for figure 6 are T_{in} = 828K, P_{in} = 1723 kPa, ϕ = 0.41. In these images, we can see ring-like structures, particularly in the OH PLIF images; these give an indication of the size and position of the flame front at this location. The PLS signal depends only on elastic scatter from droplets, whereas the fuel PLIF signal arises from both liquid and vapor. Thus, comparing the PLS and fuel PLIF images tells us whether a significant portion of the fuel is vapor or liquid. From the images in figure 5, we observe that a significant fraction of the fuel is still in the liquid phase. In contrast, the images in figure 6, acquired at higher temperature and pressure, show that the fuel is almost completely vaporized under these conditions supported by the complete lack of PLS signal arising from scatter from fuel droplets while still observing PLIF signal from fuel vapor.

We also find that for inlet temperatures above 700K, the fuel reacts within a short distance from the injector exit plane. This can be seen in a representative side view image of fuel fluorescence, shown in figure 7, in which the signal drops below 10% within the first 7 mm.

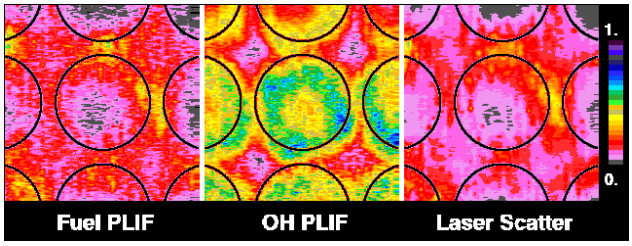

Figure 5. End views 7.5-mm from the injector exit plane showing the species pattern of total fuel (left), OH (center) and liquid fuel (right). The field of view is approximately the central 46-mm x 46-mm (of 76-mm x 76-mm). Each species is self-scaled within its entire volume. Inlet conditions: T = 617K, P = 1034 kPa, ϕ = 0.38, equal fuel split.

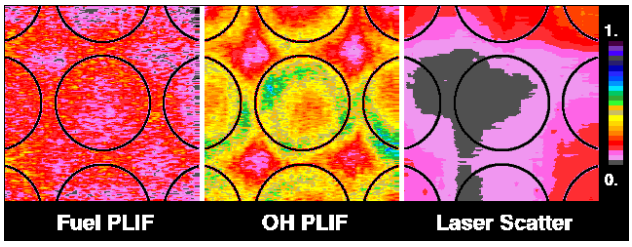

Figure 6. End views 7.5-mm from the injector exit showing the species pattern of total fuel (left) and liquid fuel (right). The field of view is approximately the central 46-mm x 46-mm (of 76-mm x 76-mm). Each species is self-scaled within its entire volume. Inlet conditions: T = 822K, P = 1724 kPa, ϕ = 0.41, equal fuel split.

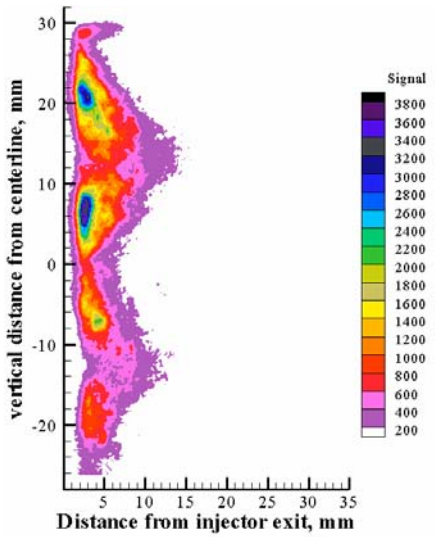

Figure 7. Center-plane slice side view of Fuel PLIF. Inlet conditions: T = 728K, P = 1034 kPa, ϕ = 0.45, equal fuel split.

Figure 8 shows a comparison of different fuel splits for the same inlet temperature, pressure and equivalence ratio of 0.35. The top row images show fuel fluorescence (left) and CH* chemiluminescence (right) with all injectors fueled equally. The second row shows the corresponding results when the fuel circuits are fed such that the four injectors centered on each side have ϕ = 0.263, while the remaining five (corners and center) have ϕ = 0.420. The bottom row shows the resultant ratio of the equal split case divided by the unequal split case. All images are focused on the center-plane. For the fuel PLIF images (left column), we observe for the unequal fuel-split case higher relative fuel flow from the center injector than from the top and bottom injectors, as expected. Likewise, the ratio shows a range from 0.7 to 0.9 in the center, which compares well with the calculated value of 0.83, and correspondingly higher values for the outer injectors. For the chemiluminescence images in the right-hand column, the converse appears to be true. However, because the CH* emissions are not induced, the resulting images are due to chemiluminescence from the bulk fluid, so we must consider the sum of each row of injectors in comparing these images. When the bulk is considered, the images are consistent with the split flows. The top and bottom rows of injectors have 5% greater flow compared to the even split case; the center injector is about 10% less.

That the PLIF ratio agrees well with calculations provides evidence that at these inlet conditions, the fluorescence signal is linear and that the field is not optically thick, which we found to be the case at some lower inlet temperature conditions. Further study and

experiments will need to be conducted to determine parameters that will indicate when flows are too optically thick to make measurements feasible.

Figure 9 shows representative CH*, NO*, and OH* chemiluminescence images acquired at two conditions where we measured the lowest and highest overall NO* signals. The images are scaled per species. Like the side view fuel PLIF image shown in figure 7, these images show that the flames are short, between 3-7 mm from the injector exit plane. In these more highly spatially-resolved images the species can be seen to emanate from the individual injectors. As expected, each species is relatively weak for the condition which gives rise to lower NO concentrations and higher for the increased inlet temperature/pressure condition.

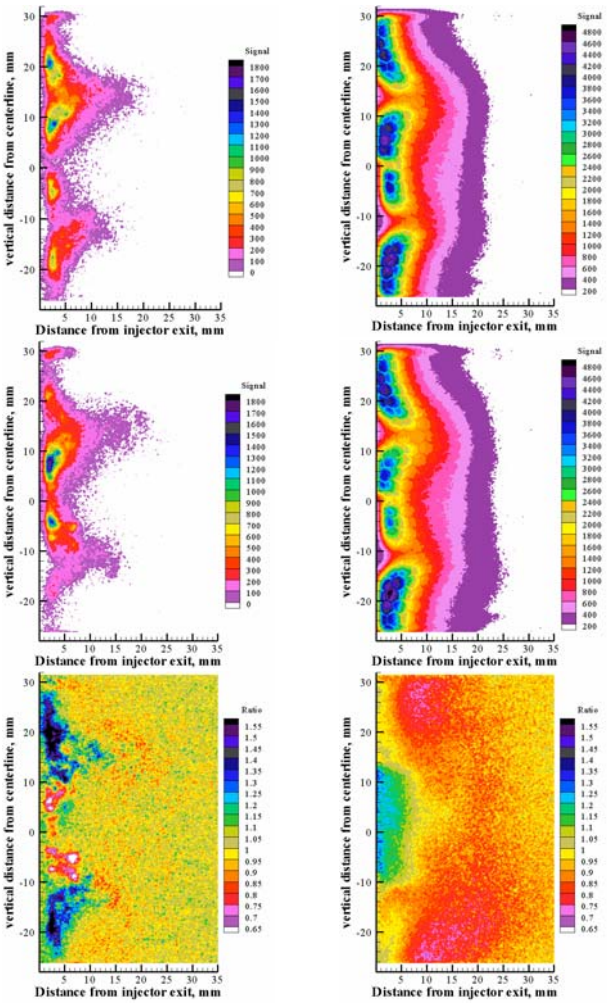

Figure 8. Examples that consider fuel staging. Left column: Fuel PLIF; Right column: CH* chemiluminescence. Top row: equal fuel split; middle row: unequal fuel split; bottom row: ratio of equal/unequal splits. Common inlet conditions: T = 728K, P = 1034 kPa, ϕ = 0.35.

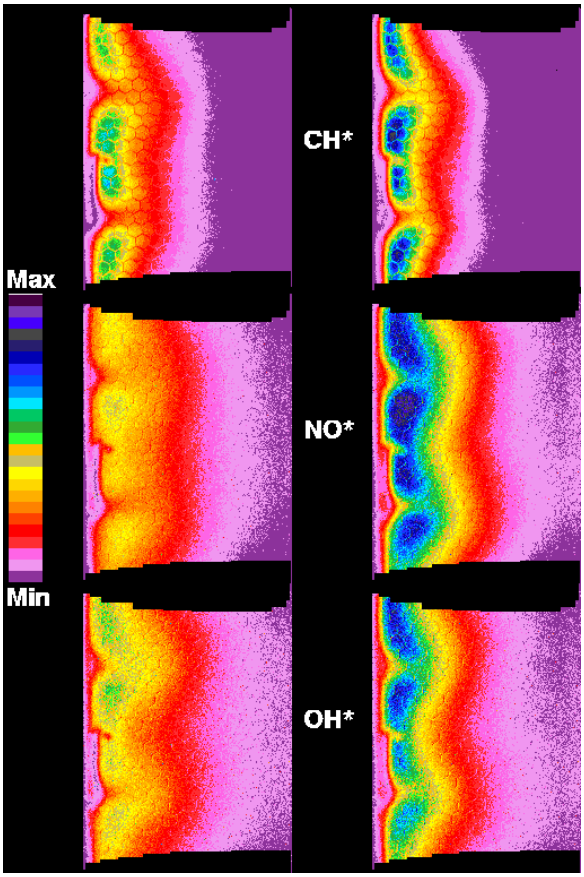

Figure 9. Chemiluminescence images of (from top) CH*, NO*, and OH* at the conditions that produce the least (left column) and most (right) NO*. Signals within each image are scaled per species. Inlet conditions: P = 1034 kPa, ϕ = 0.45, equal fuel split. T = 617 K and 828 K, respectively for left and right columns.

Figure 10 plots the various chemiluminescence or PLIF signals versus distance from the fuel injector. The data plotted are the total signal from a 0.3-mm-wide vertical "probe" sampled from the data block at fixed intervals downstream of the injector inlet. Mindful that the chemiluminescence images correspond to light emitted from the bulk volume, we simulated this effect for the PLIF data by adding the values from all forty-seven images at the corresponding axial stations.

In comparing the various species' signals, we find that the CH* and fuel PLIF signals show similar trends, which one should expect because CH* arises from the fuel side of the flame. Likewise, because NO* is primarily formed at higher temperatures and OH* is an indicator of chemical reaction and heat release, it is reasonable for the OH PLIF, OH* and NO* chemiluminescence signals to agree quite well when ranked from high to low dependent on inlet flows.

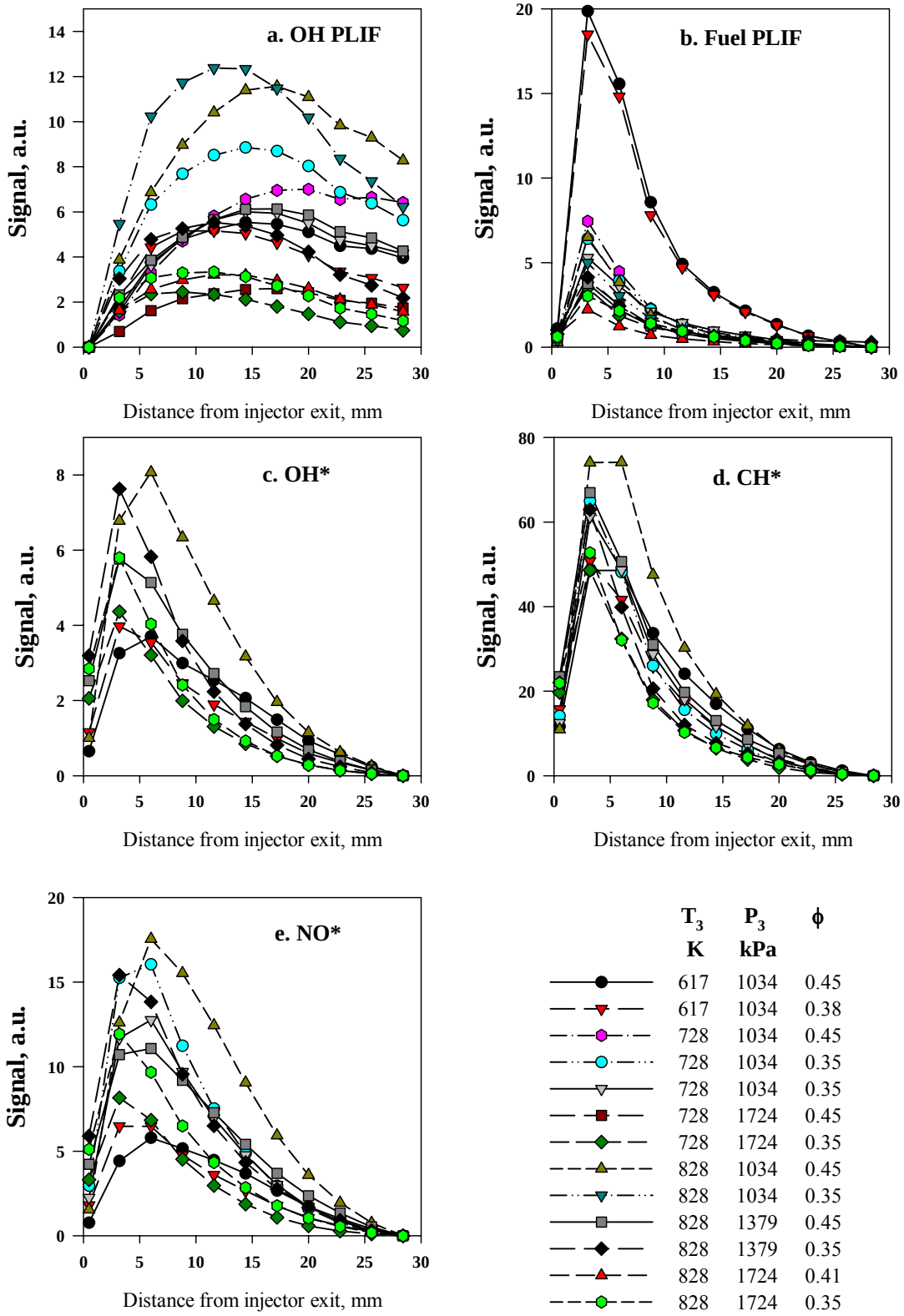

Figure 10. Plots of fuel-flow normalized chemiluminescence and PLIF data at different axial locations for a range of inlet conditions.

One key difference between the two OH decay mechanisms (figures 10a and 10c) is that the chemiluminescence data better reflect the length of the primary combustion zones whereas the OH PLIF data show that secondary reactions persist farther downstream. Since OH PLIF is a good indicator of bulk temperature, it can be used to assess temperature uniformity. In an earlier test of a similar 9-pt injector, we compared the effect of air swirl on the flow field [4]. We obtained data using 45°, 60°, and an alternating combination of 45° and 60° swirlers. Figure 11 highlights the OH PLIF results obtained in the vertical center-plane approximately 150-mm downstream of the injector, which generally corresponds to the combustor exit/turbine inlet. Insofar as bulk OH signal is an indicator of temperature, the OH images can be used to visualize the turbine temperature profile factor. In this figure, we overlay our images on diagrammatic representations of the combustor flame tube. The top diagram shows the OH Profile using 45° axial swirlers, in which we found that the OH signal was nearly twice as high as the signal in the center Therefore, greater temperature lies along the combustor walls rather than in the center, resulting in a poor turbine inlet temperature profile. We found the alternating combination of swirlers to provide the best profile, as illustrated in the bottom diagram which shows a very uniform profile.

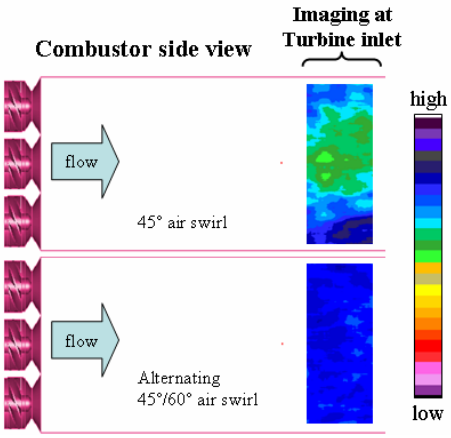

Figure 11. Swirl angle effect on turbine inlet temperature profile. Inlet conditions: 866 K, 1034 kPa, $\phi = 0.53$

Figures 12 and 13 show "cold flow", unfueled, air velocities measured at T_{in} = 617K, P_{in} = 1034 kPa, which corresponds to the fueled, combusting case species distributions shown in figure 5. Figure 12 shows the vertical and axial components of velocity along the vertical center plane. From this, we see recirculation zones immediately downstream of the fuel injectors (at vertical distances of roughly +25-mm, 0, and -25-mm), which extend approximately 17-mm downstream. The largest negative velocity occurs 5-7 mm downstream. Two small eddies between the injector sites are also observed in the image. High positive velocities begin in the region between the injection sites, with the highest velocities approximately 25-30 mm downstream of the exit plane. Figure 13 shows end view contours of axial velocity, ranging between 3-mm to 19-mm from the injector exit. From these, we find that the heart of the flow recirculation zone occurs between 5-mm to 7-mm downstream from the exit plane. These end views provide confirmation that the recirculation zones occur immediately downstream of each injection site. When comparing this velocity pattern with the species patterns of figure 6, it is clear that the primary combustion, observed in the OH PLIF images, takes place along the perimeter of the recirculation zones, with any remaining unburnt fuel being carried downstream in the regions between the injectors. Moving further downstream, we find that by approximately 19-mm all flow is positive.

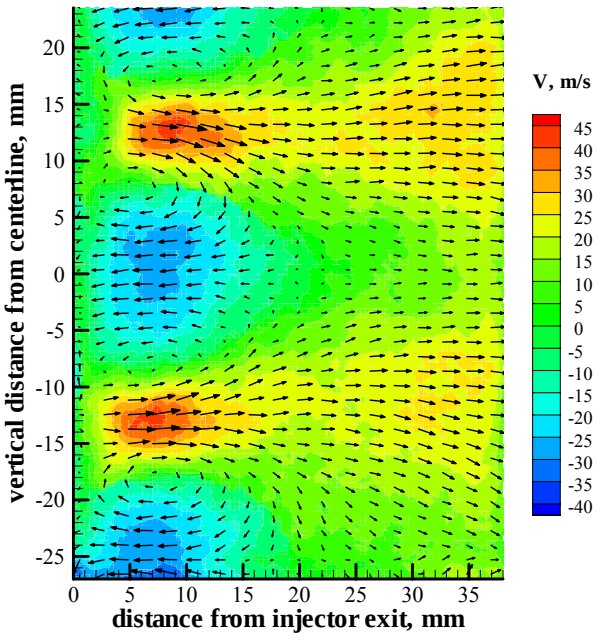

Figure 12. A side view plot showing the average axial and vertical velocity components in the central vertical plane. T_{in} = 617K, P_{in} = 1024 kPa, $\Delta P/P$ = 4%. Flow is from left to right. The x-axis denotes distance from the injector exit plane. The y-axis denotes the vertical distance above or below the test rig centerline. The velocity magnitudes are represented by contours and the direction by arrows.

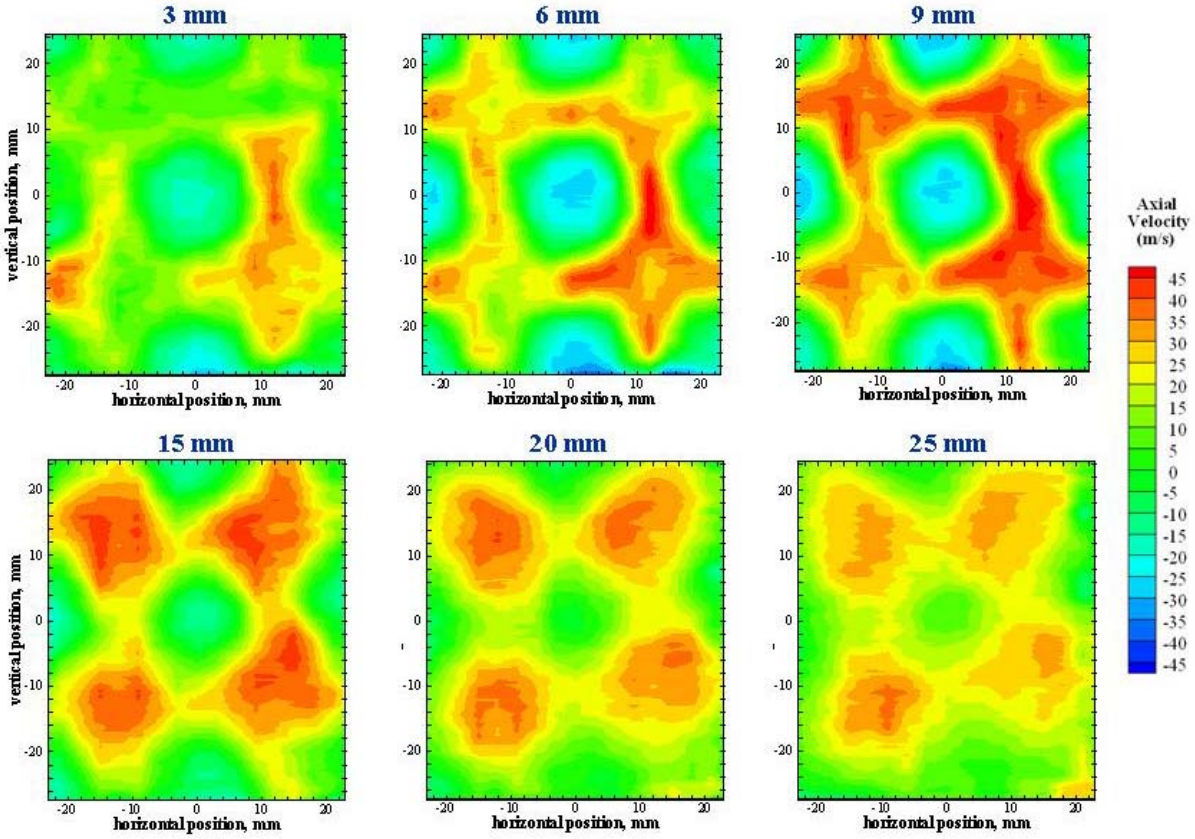

Figure 13. A series of end views ranging from 3mm to 19 mm downstream from the injector exit plane showing axial velocity contours. Experimental inlet conditions: T_{in} = 617K, P_{in} = 1034 kPa.

Figure 14 shows a comparison 6 mm downstream between experimentally– and computationally–derived axial air velocities under non-fueled, non-reacting conditions. The computations were obtained using a Reynolds-Averaged Navier Stokes (RANS) simulation [5]. Although the inlet temperature and pressure are significantly different, the trends are similar. The square overlay on the computational result shows the region accessible by our PIV experiment. The overall structure of the air velocity contours is quite similar. The regions immediately downstream of the injection points are marked by high negative velocities in each instance, and the inter-injector regions marked by high positive velocities.

CONCLUSIONS

We have presented experimental results obtained to characterize an LDI injector with the ultimate purpose of using the data to validate the National Combustion Code. These are the first of a series of experiments designed to generate a database containing both vector and scalar measurements of properties appropriate to provide fluid dynamics, mixing, fuel vaporization, chemistry and kinetics information required for CFD code development and validation. PLIF images of fuel and OH* were compared with similar images of PLS from fuel droplets at selected distances downstream of the injector exit plane. These images show that this 9-point injector array is quite uniform in the fuel distribution and atomizes and vaporizes the fuel quickly and efficiently. We found that chemiluminescence images from bulk OH* and CH* were good for visualizing the flames and overall symmetry; and better than OH PLIF for indicating the location of the primary reaction zone. PIV results are also presented that show the presence of relatively high velocity recirculation zones, predicted by NCC, immediately downstream of the fuel injection locations. A comparison of the axial air velocity from experiment and NCC code is made showing a strong general agreement even with disparate conditions.

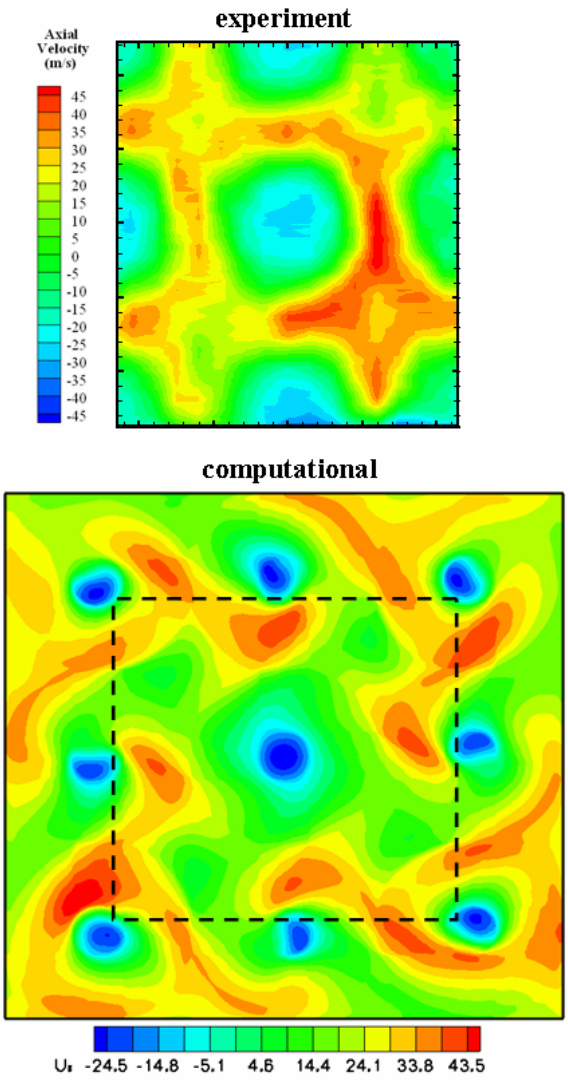

Figure 14. A comparison between experimental (top) and computationally derived (bottom) axial air velocities 6-mm downstream of the injector exit plane. Experimental inlet conditions: T_{in} = 617K, P_{in} = 1034 kPa; Computational inlet conditions: T_{in} = 822K, P_{in} = 2740 kPa. The computational results are from [5].

ACKNOWLEDGEMENT

The authors thank Robert Tacina and Changlie Wey for their assistance and guidance. We thank Farhad Davoudzadeh for providing computational results. We also thank the CE-5 test crew: Susan Adkins, Wade Arida, Ronnie Foster, Jeff Hamman, Dean Kocan, Gwynn Severt, Dawn Sgro, Richard Spangle.

REFERENCES

[1] Tacina, R., Wey, C, Laing, P., Mansour, A., 2002: *Sector Tests of a Low-NOx, Lean Direct Injection, Multipoint Integrated Module Combustor Concept*, Proceedings of ASME Turbo Expo 2002, GT-2002-30089, Amsterdam, The Netherlands.

[2] Tacina, R., Mao, C.-P., Wey, C., 2003: *Experimental Investigation of a Multiplex Fuel Injector Module for Low Emission Combustors*, Proceedings of the 41st Aerospace and Sciences Meeting and Exhibit, AIAA 2003-0827, Reno NV.

[3] Tacina, R., Lee, P., Wey, C., 2005: *A Lean-Direct-Injection Combustor Using a 9 Point Swirl-Venturi Fuel Injector*, Proceedings of ISABE, ISABE-2005-1106, Munich, Germany.

[4] Locke, R.J., Hicks, Y.R., Anderson, R.C., Ockunzzi, K.A., 1996: *OH Imaging in a Lean Burning High-Pressure Combustor*, AIAA Journal, Vol.34, No. 3, pp. 662-664.

[5] Davoudzadeh, F., Liu, N.-S., and Moder, J.P., 2006: *Investigations of Swirling Air Flows Generated by Axial Swirlers in a Flame Tube*, Proceedings of ASME Turbo Expo 2006, GT-2006-91300, Barcelona, Spain.